A stored energy analysis of grains with shear texture orientations in Cu-Ni-Si and Fe-Ni alloys processed by high-pressure torsion

Hiba Azzeddine [a,*], Thierry Baudin [b], Anne-Laure Helbert [b], François Brisset [b], Yi Huang [c,d], Megumi Kawasaki [e], Djamel Bradai [f], Terence G. Langdon [d]

[a] Faculty of technology, University of Mohamed Boudiaf, M'sila, Algeria
[b] Université Paris-Saclay, CNRS, Institut de Chimie Moléculaire et des Matériaux d'Orsay, 91405 Orsay, France
[c] Department of Design and Engineering, Faculty of Science and Technology, Bournemouth University, Poole, Dorset BH12 5BB, UK
[d] Materials Research Group, Department of Mechanical Engineering, University of Southampton, Southampton SO17 1BJ, UK
[e] School of Mechanical, Industrial and Manufacturing Engineering, Oregon State University, Corvallis, OR 97331, USA
[f] Laboratory of Materials Physics, Faculty of Physics, University of Sciences and Technology - Houari Boumediene (UST.H.B.), P.O. Box 32, El-Alia, Bab-Ezzouar DZ-16111, Algiers, Algeria

ARTICLE INFO

ABSTRACT

Experiments were conducted to evaluate the evolution of the stored energy in grains with shear texture orientations A_1^* {111}<$\bar{1}\,\bar{1}2$>, A_2^* {111}<$1\bar{2}1$>, A {111}<$1\bar{1}0$>, $\bar{A}$ {111}<$0\bar{1}1$>, B {112}<$1\bar{1}0$>, $\bar{B}$ {112}<$1\bar{1}0$> and C {100}<110> for Cu-2.5Ni-0.6Si and Fe-36Ni (wt%) alloys after high-pressure torsion (HPT) processing up to 10 turns at ambient temperature using a Kernel Average Misorientation (KAM) approach. A typical stable shear texture developed in the Cu-2.5Ni-0.6Si alloy immediately after 1 turn whereas there was a continuous transformation of texture in the Fe-36Ni alloy up to 10 turns. The results show that HPT processing produces similar stored energies of ~35 J/mol and ~24 J/mol but with different shear texture components for the Cu-2.5Ni-0.6Si and the Fe-36Ni alloy, respectively. The stored energy in all shear components for the Cu-2.5Ni-0.6Si alloy increases with increasing HPT processing up to 1 turn and then slightly decreases through 10 turns. By contrast, the stored energy of the Fe-36Ni alloy continuously decreases with increasing numbers of HPT turns. These evolutions are examined with reference to the initial textures, dynamic recrystallization, grain refinement mechanisms and differences in the stacking fault energies.

© 2020 Elsevier B.V. All rights reserved.

1. Introduction

It is well known that crystallographic texture significantly controls the anisotropy of mechanical properties and the formability during the thermo-mechanical processing of metallic alloys [1]. Generally, the orientations of the deformed grains depend on the specific deformation processing such as rolling, extrusion or torsion. In practice, a rolling texture, including the Copper {112}<11$\bar{1}$>, S {123}<634>, Brass {110}<1$\bar{1}$2>, Goss {110}<001> and Cube {100}<001> components, was widely reported in face-centered cubic (FCC) alloys processed by conventional rolling and severe plastic deformation by accumulative roll-bonding (ARB) [2,3]. By contrast, shear textures composed of A_1^* {111}<$\bar{1}\,\bar{1}2$>, A_2^* {111}<$1\bar{2}1$>, A {111}<$1\bar{1}0$>, $\bar{A}$ {111}<$0\bar{1}1$>, B {112}<$1\bar{1}0$>, $\bar{B}$ {112}<$1\bar{1}0$> and C {100}<110> were formed

during equal-channel angular pressing (ECAP) and high-pressure torsion (HPT) processing of several FCC alloys [4–6].

The development of a deformation texture in rolled FCC alloys depends strongly on the stacking fault energy (γ_{SFE}) of the processed alloys. The deformation texture after conventional rolling is classified into three categories depending on the value of γ_{SFE}. First, the deformation texture of alloys with low γ_{SFE}, such as a Cu-30Zn alloy (γ_{SFE} = 14 mJ/m^2), is characterized by a dominant Brass {110}<1$\bar{1}$2> component known as a Brass-type texture. Second, for alloys with high γ_{SFE}, such as aluminum (γ_{SFE} = 160 mJ/m^2), the Copper {112}<11$\bar{1}$> and S {123}<634> components are often dominant and this is known as a Copper-type texture. Third, it is generally assumed that the texture of alloys with medium γ_{SFE}, such as copper (γ_{SFE} = 78 mJ/m^2) and an Fe-Ni alloy (γ_{SFE} ~ 122 mJ/m^2), contains Copper, S and Brass components in fairly equal fractions.

Nevertheless, the evolution of a deformation texture in alloys with medium γ_{SFE} is complicated and no definitive trends exist in texture evolution. For example, while cold rolling of Fe-36Ni alloy samples leads to the formation of a typical copper texture with the

* Corresponding author.
  E-mail address: hiba.azzeddine@univ-msila.dz (H. Azzeddine).

H. Azzeddine, T. Baudin, A.-L. Helbert et al.

presence of Copper, S and weak Brass components [7], the deformation textures of cold-rolled Cu-2.7Ni-0.6Si (wt%) and Cu-15Ni-8Sn (wt%) alloys, having medium γ_{SFE} (~50 mJ/mol for the Cu-15Ni-8Sn alloy), show dominant Brass components which are typical for alloys with low γ_{SFE} [8,9]. It has been also shown that the Brass component might strengthen with increasing deformation strain due to the presence of twins that produces a re-orientation of the Copper component to a Brass component [8]. Moreover, it is reasonable to expect that the recrystallization texture of medium to high γ_{SFE} alloys may be characterized by the formation of a Cube {100}<001>texture but many experiments have shown the deformation texture is retained after annealing of the cold-rolled Cu-15Ni-8Sn alloy [9]. Accordingly, it was concluded that the deformation and recrystallization textures of alloys with medium γ_{SFE} strongly depend on the nature of the deformation processing and the chemical composition of the alloy.

In investigations of the deformation textures, it was demonstrated that the numbers of dislocations stored within the grains was dependent upon the local crystallographic orientation [10–12]. In practice, the stored energy in deformed grains of different orientations plays a significant role in controlling the onset of recrystallization and the corresponding texture development [11].

Generally, the total dislocation density is composed of two types: geometrically necessary dislocations (GNDs) and statistically stored dislocations (SSDs) [13]. The stored energy related to the Brass {110}<1$\bar{1}$2>, Copper {112}<11$\bar{1}$>, S {231}<346> and Cube {001}<100>texture components of several FCC alloys was investigated after conventional rolling and ARB [10–12,14,15]. A hierarchy was found in several processed alloys whereby the stored energy, E, of the texture components varied as $E_{Copper} > E_S > E_{Brass} > E_{Cube}$ [11,12,15]. It was suggested that the orientated grains with high energy were rapidly replaced by Cube grains (with low energy) during annealing treatments [11,12]. The stored energy in the oriented grains in an ARB-processed Fe-36Ni alloy was found to fluctuate (specifically, to decrease and subsequently to increase) upon increasing the numbers of ARB processing passes due to the occurrence of dynamic recrystallization (DRX), the formation of fine grains and the production of new dislocations [11]. In addition, it was demonstrated that the GNDs in the cells/sub-grain walls are responsible for the increase in the stored energy during ARB processing [11]. The GNDs also contributed significantly to the bulk stored energy of the HPT-processed Cu-2.5Ni-0.6Si alloy at equivalent strains in the range of ~8.6–16 and afterwards this contribution slightly decreased due to the occurrence of DRX and the formation of fine grains [16]. The evolution of the shear texture components by HPT processing as a function of the γ_{SFE} of alloys is rarely documented in published reports and no systematic investigation has been undertaken to evaluate the stored energy in the shear texture oriented grains.

In fact, it is only known that the Taylor factor in the different shear texture components increases in the following order: $A/\bar{A} < A_1^*/A_2^* < B/\bar{B} < C$ [17,18]. The Taylor factor is defined as the total slip amplitude corresponding to a unit macroscopic strain increase [17,19]. Consequently, it may be suggested that a grain with high Taylor factor has higher dislocation density and hence high stored energy [20,21]. However, a direct correlation between the Taylor factor and the stored energy is not yet established.

Based on the limited data available to date, the present study was initiated in order to quantify the stored energy and thereby to clarify its relationship with the shear texture components for Cu-2.5Ni-0.6Si and Fe-36Ni alloys after HPT processing at room temperature for ½, 1 and 10 turns using a Kernel Average Misorientation (KAM) approach. The effect of γ_{SFE} on the stored energy is also examined. It must be noted that the stored energy estimated in the present study arose from the GND dislocations since the KAM approach allows only an estimation of this type of dislocation [16,22]. Full details on the

evolution of the texture and the microstructural parameters, such as grain size and grain boundary orientation distributions, of the HPT-processed Cu-2.5Ni-0.6Si and Fe-36Ni alloys were given in earlier reports [5,6] and therefore the present investigation was undertaken to provide a special emphasis on the stored energy and the shear texture component correlations.

2. Experimental materials and procedures

The Cu-2.3Ni-0.5Si (wt%) and Fe-36Ni (wt%) alloys were supplied by CLAL-MSX (Meru, France) and APERAM Alloys Imphy Society, France, respectively. Accordingly, the Cu-2.3Ni-0.5Si alloy was provided in supersaturated solid-solution condition after casting and hot rolling at 830 °C whereas, the Fe-36Ni sheet alloy was provided in a fully recrystallization state. Both alloys were machined into disks having diameters of 10 mm and thicknesses of ~0.85 mm. The HPT processing was performed at ambient temperature through totals, N, of 1/2, 1, 5 and 10 turns using an imposed pressure of 6.0 GPa and a rotational speed of 1 rpm under quasi-constrained conditions [23].

The microstructure and microtexture were analysed using a scanning electron microscope FEG-SEM SUPRA 55 VP operating at 20 kV with TSL Orientation Imaging Microscopy, OIM™ software. The electron backscatter diffraction (EBSD) measurements were performed in the RD-SD plane of the processed discs where RD and SD denote the rotational and shear directions, respectively, after mechanical and electrolytic polishing at ambient temperature using an A2 Struers electrolyte at 24 V for 20 s (for Cu-2.5Ni-0.6Si alloy) and at 30 V for 12 s (for Fe-36Ni alloy). The presentation of the axis system and the EBSD position measurement on the disk is illustrated in Fig. 1. The EBSD maps were collected at the mid-radius (r = 2.5 mm, as shown in Fig. 1) of each disk on a 25 × 25 µm² area using a step size of 25 nm for the Cu-2.5Ni-0.6Si alloy and a 50 × 50 µm² area with a step size of 50 nm for the Fe-36Ni alloy. An area of 100 × 100 µm² was used with step sizes of 1 and 0.1 µm for the initial states of the Cu-2.5Ni-0.6Si and Fe-36Ni alloys, respectively. A grain tolerance angle of 5° and a minimum grain size of 2 pixels were chosen to obtain the grain size data. All datum points with a confidence index (CI) lower than 0.05 were excluded from the analysis where CI quantifies the reliabilities of the indexed patterns [24].

A quantitative texture analysis was carried out by calculating the Orientation Distribution Function (ODF) using MTex software [25]. The recalculated {111} pole figures were determined using the harmonic method (L = 22) with each orientation modeled with a Gaussian function having a half-width of 5°. Usually, the KAM approach allows quantifying the dislocation density belonging to the GNDs type and the corresponding stored energy in the microstructure by the following equations [15,26]:

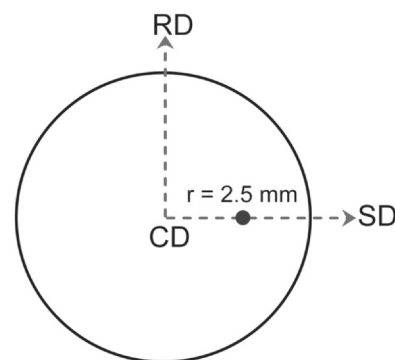$$\rho = \frac{\alpha \theta_{KAM}}{ndb} \tag{1}$$

Fig. 1. Illustration of axis system of the processed disc for the EBSD measurement. SD, RD and CD correspond to the shear, rotation and compression directions, respectively.

$$E_{KAM} = \frac{1}{2}\rho\mu b^2 = \frac{\mu b \theta_{KAM}}{2d} \qquad (2)$$

where α is a parameter which depends on the grain boundary type with values of 2 and 4 for pure tilt and twist boundaries, respectively [27], θ_{KAM} is the misorientation angle, b the magnitude of the Burgers vector (b = 0.255 and 0.253 nm for Cu-2.5Ni-0.6Si and Fe-36Ni, respectively), n = 3 for the nearest neighbor, d the EBSD scan step size, and μ the shear modulus having values of 48.3 and 57 GPa for copper and iron, respectively. The θ_{KAM} value was calculated from the mean misorientation angle between the point and its third neighbor excluding misorientations greater than 5°. It may be preferable to increase the CI to 0.1 since the samples undergo SPD processing and to ensure the reliability of the EBSD scans. However, the difference between the two clean-up procedures was very small and $\Delta\theta_{KAM}$ = 0.01°. In practice, it is better for comparison to use the normalized KAM (KAM$_{nor}$ = θ_{KAM}/nd) parameter since the EBSD step sizes for both alloys are not the same [11].

The grain orientation spread (GOS) approach implemented in the OIM™ software is used to separate the recrystallized grains from the deformed grains where GOS is defined as the average deviation between the orientation of each point in the grain and the average orientation of the grain [28]. In this research, grains were considered recrystallized if the value of GOS was lower than 1° [28].

3. Experimental results

Fig. 2 shows (a) and (b) the KAM maps and (c) and (d) the recalculated {111} pole figures for the as-received Cu-2.5Ni-0.6Si and Fe-36Ni alloys, respectively. The positions of the main ideal rolling texture components for FCC alloys are listed in Table 1. The normalized KAM value of 1.3°/μm for Cu-2.5Ni-0.6Si is relatively higher than 0.8°/μm for Fe-36Ni as shown in the upper regions of the KAM maps indicating high dislocation densities. Both alloys exhibit microstructures with equiaxed grains containing high fractions of twins (Σ3 60° < 111 >) as can be seen by the arrows. The mean grain sizes

Table 1
Main ideal rolling and shear texture components of FCC alloys.

Component	{hkl} < uvw >	Euler Angle		
		φ_1	ϕ	φ_2
■ Brass	{110} < 1$\bar{1}$2 >	54.7°	90°	45°
● Cube	{001} < 100 >	0°	0°	0°
▲ Copper	{112} < 11$\bar{1}$ >	270°	35°	45°
♦ S	{123} < 634 >	59°	36.7°	63.4°
△	{111} < $\bar{1}\bar{1}$2 >	90°	54.74°	45°
▽	{111} < 1$\bar{2}$1 >	30°	54.74°	45°
◯ A	{111} < 1$\bar{1}$0 >	0°	54.74°	45°
◯ $\bar{A}$	{111} < 0$\bar{1}$1 >	60°	54.74°	45°
▢ B	{112} < 1$\bar{1}$0 >	0°	35.26°	45°
◇ $\bar{B}$	{112} < $\bar{1}$10 >	180°	35.26°	45°
◯ C	{001} < 110 >	45°	0°	0°

were determined without considering twins and the results gave ~20 μm for Cu-2.5Ni-0.6Si and ~10 μm for Fe-36Ni, respectively. The Copper, S and Brass components were equally present for the as-received Cu-2.5Ni-0.6Si alloy where it is a typical texture for rolled FCC alloys having medium values of γ_{SFE}. By contrast, a typical recrystallization texture with a dominant Cube component was observed for the as-received Fe-36Ni alloy while a weak Brass component is evident in the {111} pole figure for this alloy. The variations in the initial microstructures and textures between these two alloys is due to differences in their manufacturing processing histories.

Figs. 3 and 4 show a series of KAM and GOS maps and the recalculated {111} pole figures of the HPT-processed Cu-2.5Ni-0.6Si and Fe-36Ni alloys after, from top, N = ½, 1, 5 and 10 turns, respectively. The KAM_{nor} values and the fractions of the recrystallized grains (F_{DRX}) for each sample are presented in the KAM and GOS maps. After N = ½ turn, the normalized KAM value increases rapidly from 1.3°/μm to 16.2°/μm for the Cu-2.5Ni-0.6Si alloy and from 0.8°/μm to 9.2°/μm

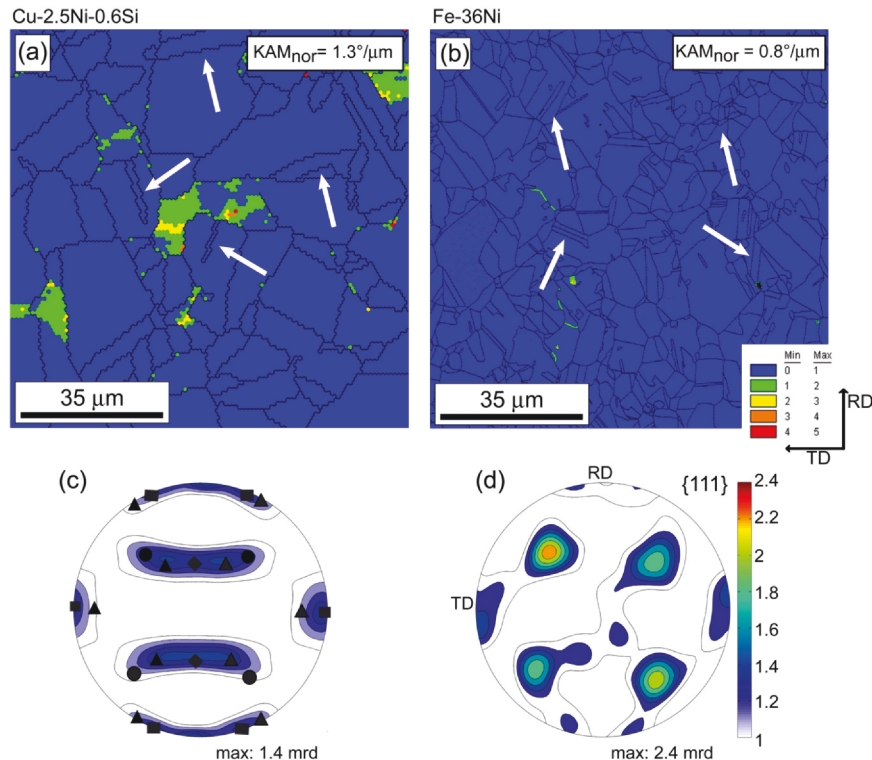**Fig. 2.** KAM maps and the recalculated {111} pole figure of the as-received: (a, c) Cu-2.5Ni-0.6Si and (b, d) Fe-36Ni alloys.

H. Azzeddine, T. Baudin, A.-L. Helbert et al.

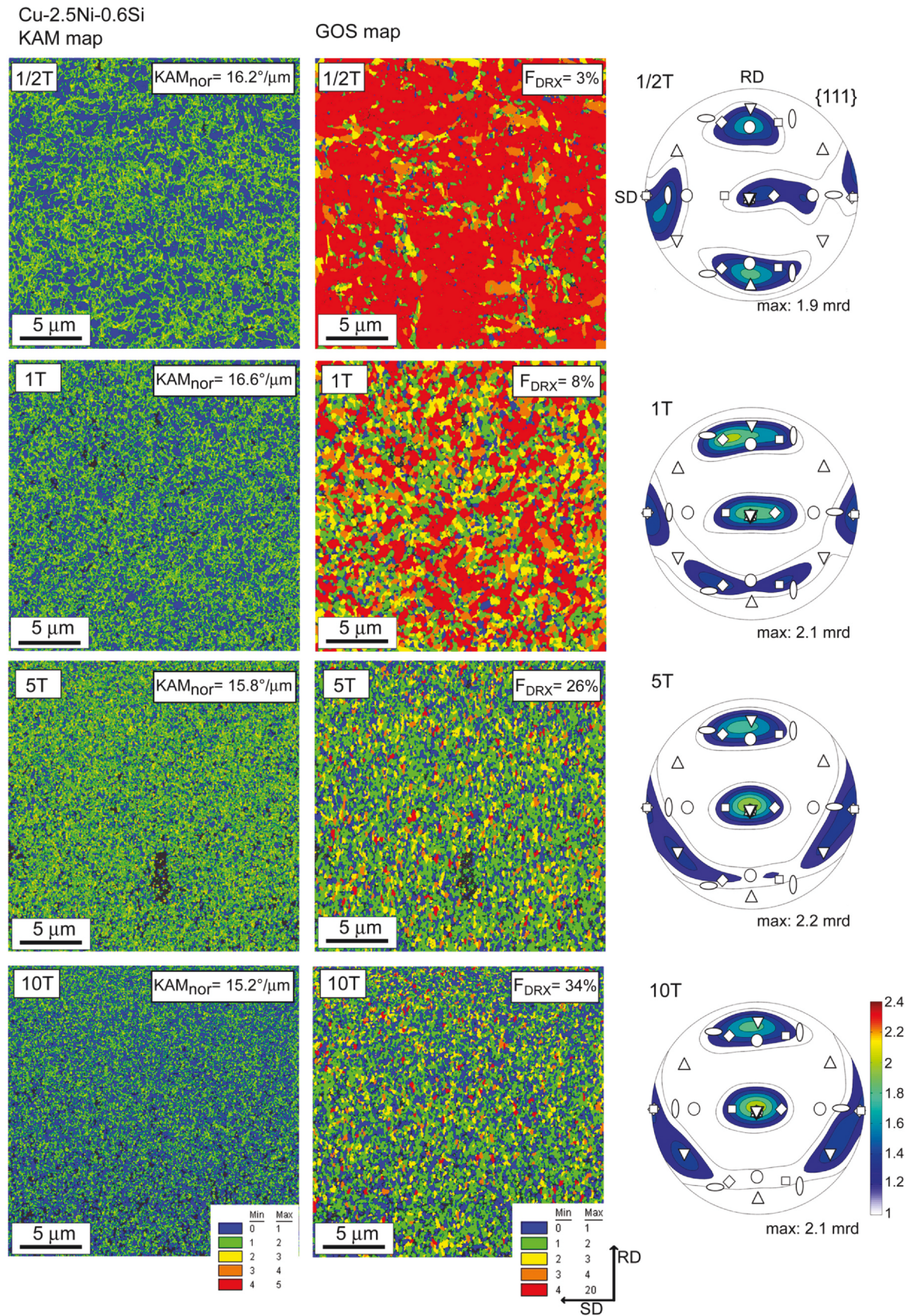**Fig. 3.** KAM, GOS maps and the recalculated {111} pole figure of the HPT processed Cu-2.5Ni-0.6Si alloy after N = ½, 1, 5 and 10 turns.

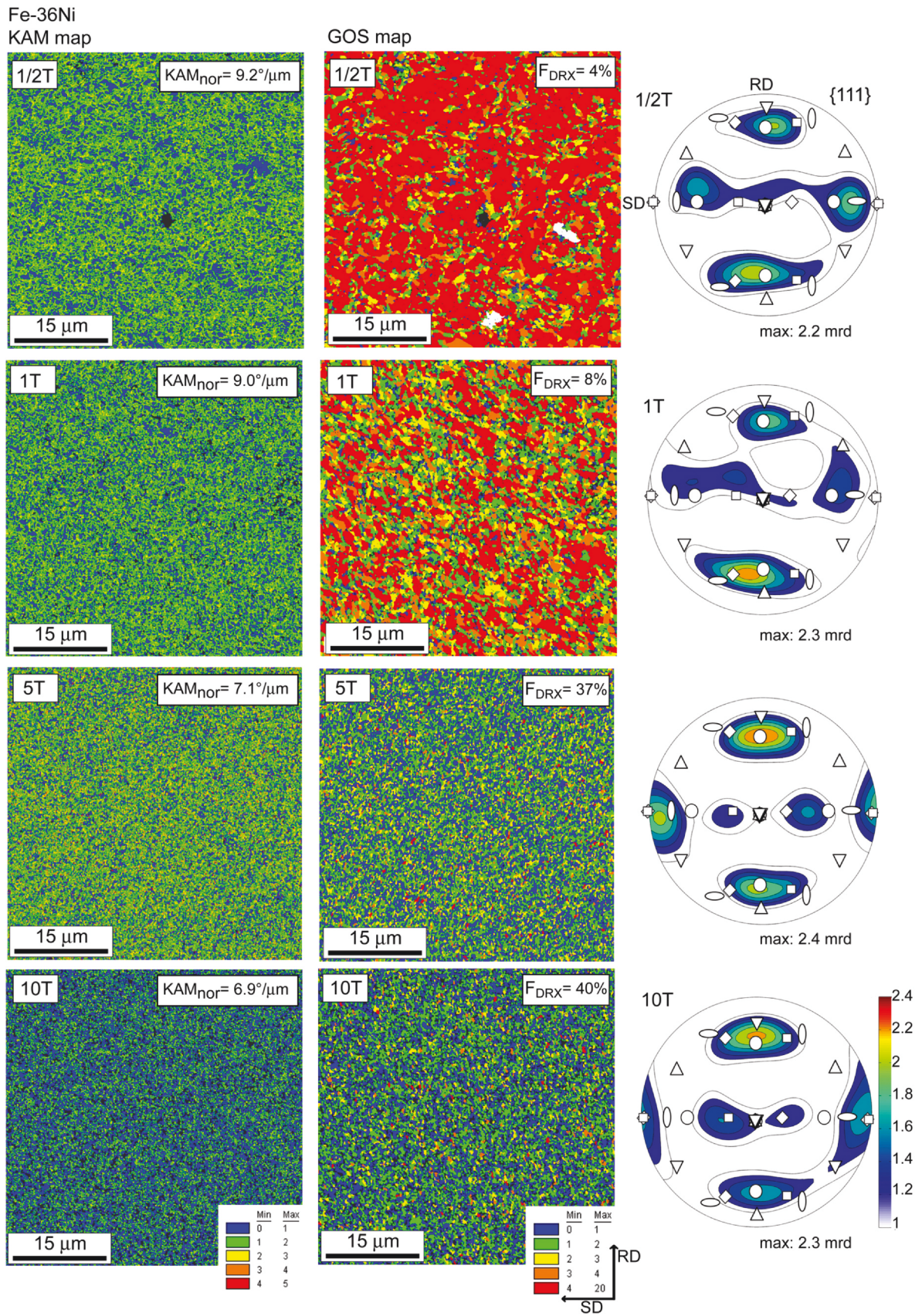**Fig. 4.** KAM, GOS maps and the recalculated {111} pole figure of the HPT processed Fe-36Ni alloy after N = ½, 1, 5 and 10 turns.

for the Fe-36Ni alloy due to the generation and accumulation of dislocations. For the Cu-2.5Ni-0.6Si alloy the normalized KAM value continues to increase to 16.6°/μm after $N = 1$ turn and then decreases to 15.2°/μm after $N = 10$ turns whereas for the Fe-36Ni alloy the normalized KAM value appears to saturate at 9°/μm after $N = 1$ turn and then continuously decreases to 6.9°/μm through $N = 10$ turns. The decrease in the normalized KAM values is accompanied by an increase in the fraction of recrystallized grains, thereby indicating the occurrence of a dynamic recrystallization process. This trend is especially evident between 1 and 5 turns for the Fe-Ni alloy. It is also noted that the fraction of DRX of 37% is higher for Fe-36Ni after $N = 5$ turns than the fraction of 26% for Cu-2.5Ni-0.6Si.

The evolution of the texture by means of the {111} recalculated pole figures as a function of the numbers of HPT turns is shown in Figs. 3 and 4 for Cu-2.5Ni-0.6Si and Fe-36Ni, respectively. The main ideal shear texture components of FCC alloys are summarized in Table 1. The A_1^*, A_2^*, B, $\bar{B}$ and C components were formed immediately after $N = ½$ turn and a typical shear texture is well-defined after $N = 1$ turn by the appearance of the A and $\bar{A}$ components for the Cu-2.5Ni-0.6Si alloy. Almost identical textures are also observed after 5 and 10 turns. By contrast, the texture evolution shows different trends for the Fe-36Ni alloy. The C, A and $\bar{A}$ components start to form initially after $N = ½$ turn but these C, A and $\bar{A}$ components tend to transform gradually into B and $\bar{B}$ components with increasing numbers of HPT turns as seen in the {111} pole figure of the sample after $N = 5$ turns. A nearly typical shear texture with the presence of most shear texture components was developed only after $N = 5$ turns and appeared to stabilize after $N = 10$ turns.

The evolution of the stored energy in the shear texture components, E_s, is shown in Fig. 5 as a function of the numbers of HPT turns for (a) Cu-2.5Ni-0.6Si and (b) Fe-36Ni alloys. In addition, the values of the dislocation density calculated from the KAM approach and used to estimate the stored energy are summarized in Table 2. After $N = ½$ turn, the A_1^* component shows the highest value of 36.6 ± 1.2 mJ/mol followed by the B component with 35.6 ± 0.3 mJ/mol for the Cu-2.5Ni-0.6Si alloy. However, this order is reversed after $N = 1$ turn where the stored energy of the B component increases to 36.9 ± 0.6 mJ/mol while it remains constant for the A_1^* component. Moreover, the stored energy for the A_2^* component remained reasonably similar from 33.1 ± 0.5 mJ/mol after $N = ½$ turn to 36.34 ± 0.7 mJ/mol after $N = 1$ turn. Processing by HPT for $N = 5$ turns led to a decrease in the stored energy for all shear components except for the A and $\bar{A}$ components. In addition, the stored energy of all shear components further decreased through $N = 10$ turns but it was less pronounced for the A and C components.

For the Fe-36Ni alloy, the A_2^* component exhibits the lowest stored energy of ~22.6 ± 0.7 mJ/mol compared to any other shear components after $N = 1/2$ turn. The stored energy of the A_2^* and C

Table 2
Evolution of the dislocation density in grains with different shear texture components as a function of number of HPT turns for Cu-2.5Ni-0.6Si and Fe-36Ni alloys.

Alloy	N	Dislocation density ($\rho \times 10^{15}$ m^2)						
		A_1^*	A_2^*	A	$\bar{A}$	B	$\bar{B}$	C
Cu-2.5Ni-0.6Si	½	3.35	3.03	3.11	3.14	3.27	3.16	3.11
	1	3.35	3.33	3.19	3.30	3.38	3.35	3.14
	5	3.22	3.11	3.22	3.30	3.16	3.16	3.08
	10	3.06	2.98	3.16	3.11	3.06	3.06	3.00
Fe-36Ni	½	1.91	1.76	1.91	1.91	1.84	1.90	1.88
	1	1.84	1.80	1.80	1.86	1.81	1.83	1.88
	5	1.33	1.42	1.40	1.34	1.49	1.49	1.45
	10	1.34	1.33	1.27	1.34	1.44	1.40	1.34

components was unchanged at ~22.5 ± 1.2 mJ/mol and ~24.0 ± 0.5 mJ/mol, respectively, after $N = 1$ turn while it decreased slightly for the remaining shear components. Thereafter, the stored energy decreased rapidly in all shear components after $N = 5$ turns. The stored energy decreased continuously to $N = 10$ turns except for a stabilization at 16.9 ± 0.8 mJ/mol and 17.1 ± 0.7 mJ/mol for the A_1^* and $\bar{A}$ components, respectively.

Generally, the amount of the stored energy was similar in the different shear texture components for both alloys and no hierarchy was formed as reported previously in an ARB-processed Fe-36Ni alloy [11]. However, close inspection shows that the C and A_2^* components exhibit the lower stored energy among all shear components for the Cu-2.5Ni-0.6Si alloy after high strains for $N = 5$ and 10 turns while the B, $\bar{B}$ and C components have the highest values for the Fe-36Ni alloy. Such high values of stored energy in grains with B, $\bar{B}$ and C components imply a relatively faster recrystallization during an annealing treatment after HPT processing.

4. Discussion

The results from this investigation demonstrate that the Cu-2.5Ni-0.6Si and Fe-36Ni alloys exhibit different microstructural evolutions after HPT processing. First, the dislocation density increases in Cu-2.5Ni-0.6Si with increasing numbers of HPT turns at $N = 1$ turn and then decreases up to $N = 10$ turns. By contrast, the dislocation density continuously decreases with increasing HPT turns through $N = 10$ turns for Fe-36Ni. Moreover, these alloys show inconsistent trends in the evolution of stored energy in the shear components as demonstrated in Fig. 5. Second, it is anticipated from the behavior of the stored energy in the different shear texture components that DRX is restricted in Cu-2.5Ni-0.6Si compared to Fe-36Ni and this is apparent especially after $N = 5$ turns. Third, a typical shear texture was formed in Cu-2.5Ni-0.6Si as early as $N = 1/2$ turn
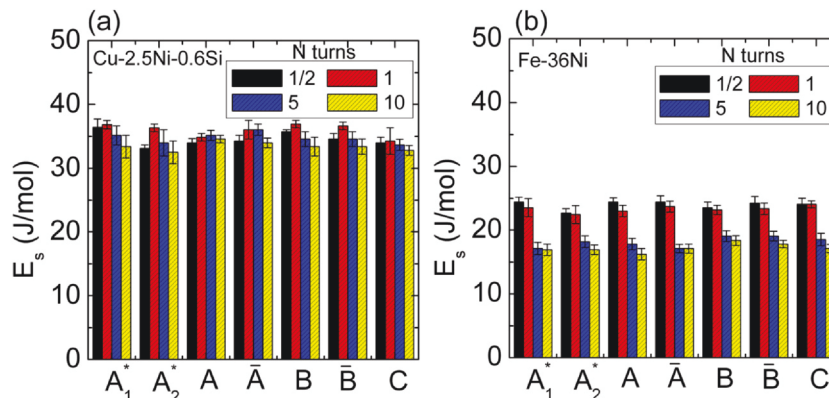

Fig. 5. Evolution of the stored energy in the shear texture components as a function of number of HPT turns of the: (a) Cu-2.5Ni-0.6Si and (b) Fe-36Ni alloy.

H. Azzeddine, T. Baudin, A.-L. Helbert et al.

and then stabilized whereas the shear component continuously developed with increasing numbers of HPT turns for Fe-36Ni. However, both alloys share a common behavior where the texture does not sharpen with increasing strain as usually observed in rolled or ARB-processed alloys [3,9]. This difference is attributed to the nature of the simple shear strain mode and the established occurrence of a strong grain subdivision during HPT processing [18].

The inconsistency in the microstructural and texture evolution between the two alloys is due to the difference in the values of their stacking fault energy, γ_{SFE}. The γ_{SFE} of the Fe-36Ni alloy was estimated from X-ray diffraction line profile analysis as ~122 mJ/m^2 [29]. The γ_{SFE} of the Cu-2.5Ni-0.6Si alloy is not at present available but it may be estimated from the relationship [30]:

$$\gamma_{SFE} = \frac{\mu a^3 \rho}{24\sqrt{3}\,\pi\alpha} \qquad (3)$$

where a is the lattice spacing and α is the net stacking fault probability. In a previously reported X-ray diffraction analysis of results of the same Cu-2.5Ni-0.6Si alloy after cold-rolling followed by annealing [31], the value of γ_{SFE} was estimated as ~64.2 mJ/m^2. It is recognized therefore that, based on the available data, the γ_{SFE} values for both Cu-2.5Ni-0.6Si and Fe-36Ni are in the medium range but the γ_{SFE} of Cu-2.5Ni-0.6Si is lower by a factor of ~2 than Fe-36Ni (thus, $\gamma_{SFE\,(CuNiSi)} \approx \gamma_{SFE\,(FeNi)}/2$).

Considering these differences, it is well known that a low γ_{SFE} promotes deformation twinning due to an insufficient dislocation system for accommodating the plastic deformation. No twins were observed in the EBSD maps for Cu-2.5Ni-0.6Si in the early stage of HPT processing for $N = 1/2$ turn although it is recognized that this may depend at least in part on limitations in the EBSD facility. In an earlier study, transmission electron microscopy (TEM) revealed the presence of twins in the same Cu-2.5Ni-0.6Si alloy after ECAP processing up to 12 passes but not after HPT processing of this alloy [32] where the absence of twins after HPT was attributed to the very small size of the twins and the limitation of conventional TEM. Twins were observed by TEM in pure copper (γ_{SFE} = 78 mJ/m^2), Cu–10 wt% Zn (γ_{SFE} = 35 mJ/m^2) and Cu–30 wt% Zn (γ_{SFE} = 14 mJ/m^2) after HPT processing for $N = 5$ turns at room temperature but it was found that the density of twins was significantly lower in pure copper compared with the Cu-Zn alloys [33]. Therefore, it is reasonable to conclude that twins are found only occasionally after the SPD processing of copper-based alloys [34].

Twinning may lead to the formation of new orientations since it causes re-orientations of the parent grains. However, the evolution of texture in the Cu-2.5Ni-0.6Si alloy was stable and no new orientations were detected with increasing numbers of HPT turns, thereby indicating the occurrence of twinning only in the very early stage of HPT processing through ½ turn. In practice, the continuous texture transformation observed for the HPT-processed Fe-36Ni alloy indicates that twinning is not the only responsible mechanism for texture modification since twinning is usually hardly activated during room temperature deformation of Fe-36Ni because of the relatively high γ_{SFE}. It was suggested earlier that dislocation generation may be hindered by grain boundaries that produce changes in the slip activity due to anisotropic hardening and hence texture modification [4]. The formation of all shear components in Cu-2.5Ni-0.6Si immediately after $N = ½$ turn retains the texture upon increasing numbers of HPT turns leading to a repetition of the deformation path. By contrast, texture stabilization was not evident in Fe-36Ni where the shear components gradually developed with increasing numbers of HPT turns and became relatively stable after 10 turns since all shear components developed during HPT processing for $N = 5$ turns.

It should be noted that the initial texture may also influence the difference in the texture evolution for both alloys especially in the early stage of deformation through N = ½ and 1 turn. Fig. 2 shows

that the initial textures of the alloys were different and, in order to examine the effect of the initial texture, a visco-plastic self-consistent (VPSC) model was used to simulate the deformed texture after torsional deformation. Details of the VPSC theory, the general formulation and the relevant algorithms are given elsewhere [35,36].

In the present study, an equivalent strain of $\varepsilon_{eq} = 5.52$ at a mid-radius of 2.5 mm in the disk sample after HPT for $N = ½$ turn was simulated by imposing successive deformation increments under a velocity gradient tensor as follows:

$$\dot{\gamma} = \begin{bmatrix} 0 & 0 & 1 \\ 0 & 0 & 0 \\ 0 & 0 & 0 \end{bmatrix} \qquad (4)$$

The equivalent stain introduced by HPT processing for $N = ½$ turn was calculated using the conventional relationship for |HPT processing [37]:

$$\varepsilon_{eq} = \frac{2\pi N r}{h\sqrt{3}} \qquad (5)$$

where r is the radial distance from the centre of the disk and h is the disk thickness equal to 0.85 mm.

The simulated texture is presented in Fig. 6 for the initial texture (upper) and the deformed texture after $N = ½$ turn (lower) for the Cu-2.5Ni-0.6Si (on left) and Fe-36Ni (on right) alloys, respectively. For comparison purposes, the textures measured in the experiments as shown in Figs. 3 and 4 for $N = ½$ turn are also given (middle). The starting texture used in the simulation was represented by 1000 orientations obtained from the initial textures of the alloys shown in Fig. 2. It was assumed that the plastic deformation was accommodated by {111} < 110 > slip systems with constant critical resolved shear stress. Inspection shows that the VPSC model provides a reasonably good representation of the main features of the experimental texture for both alloys after HPT processing for 1/2 turn and this demonstrates that the initial texture is responsible for the differences in the textures developed through HPT processing between the Cu-2.5Ni-0.6Si and Fe-36Ni alloys.

In practice, the presently studied alloys fail to exhibit a stored energy evolution that follows any systematic hierarchy depending on the texture components as found earlier in the rolling textures of an ARB-processed Fe-36Ni alloy [11]. As shown in Fig. 5, all shear components in both alloys stored similar densities of dislocations at any numbers of HPT turns. This may be due to the very large strain introduced by HPT processing that activates all populations of the {111} < 110 > slip systems in all deformed grains having various orientations. However, in practice the values of the stored energy in the Cu-2.5Ni-0.6Si alloy are higher than in the Fe-36Ni alloy for all shear texture components and this indicates that Cu-2.5Ni-0.6Si contains a higher dislocation density than Fe-36Ni. This is expected since the SPD processing of alloys with low γ_{SFE} produces a high degree of dislocation dissociation that subsequently hinders their annihilation and consequently leads to very large dislocation densities [38]. In addition, the stored energy in all shear components continuously decreases with increasing numbers of HPT turns for the Fe-36Ni alloy whereas the reduction starts only after 5 turns for the Cu-2.5Ni-0.6Si alloy. This indicates that the rate of dislocation annihilation in the Cu-2.5Ni-0.6Si alloy is relatively low compared to the Fe-36Ni alloy.

The low value of the γ_{SFE} means that the recombination and cross-slip of dissociated dislocations is difficult, thereby delaying the recovery and dynamic recrystallization processes [33]. This is in good agreement with the evolution of the DRX fraction shown in Figs. 3 and 4 where the fraction of DRX was relatively high in the Fe-36Ni alloy compared to the Cu-2.5Ni-0.6Si alloy, especially after $N = 5$ and 10 turns. Thus, the recovery and DRX processes take place after $N = 5$ turns ($\varepsilon_{eq} = 53.3$) for the Cu-2.5Ni-0.6Si alloy but this occurs as early as after $N = 1$ turn ($\varepsilon_{eq} = 10.6$) for the Fe-36Ni alloy.

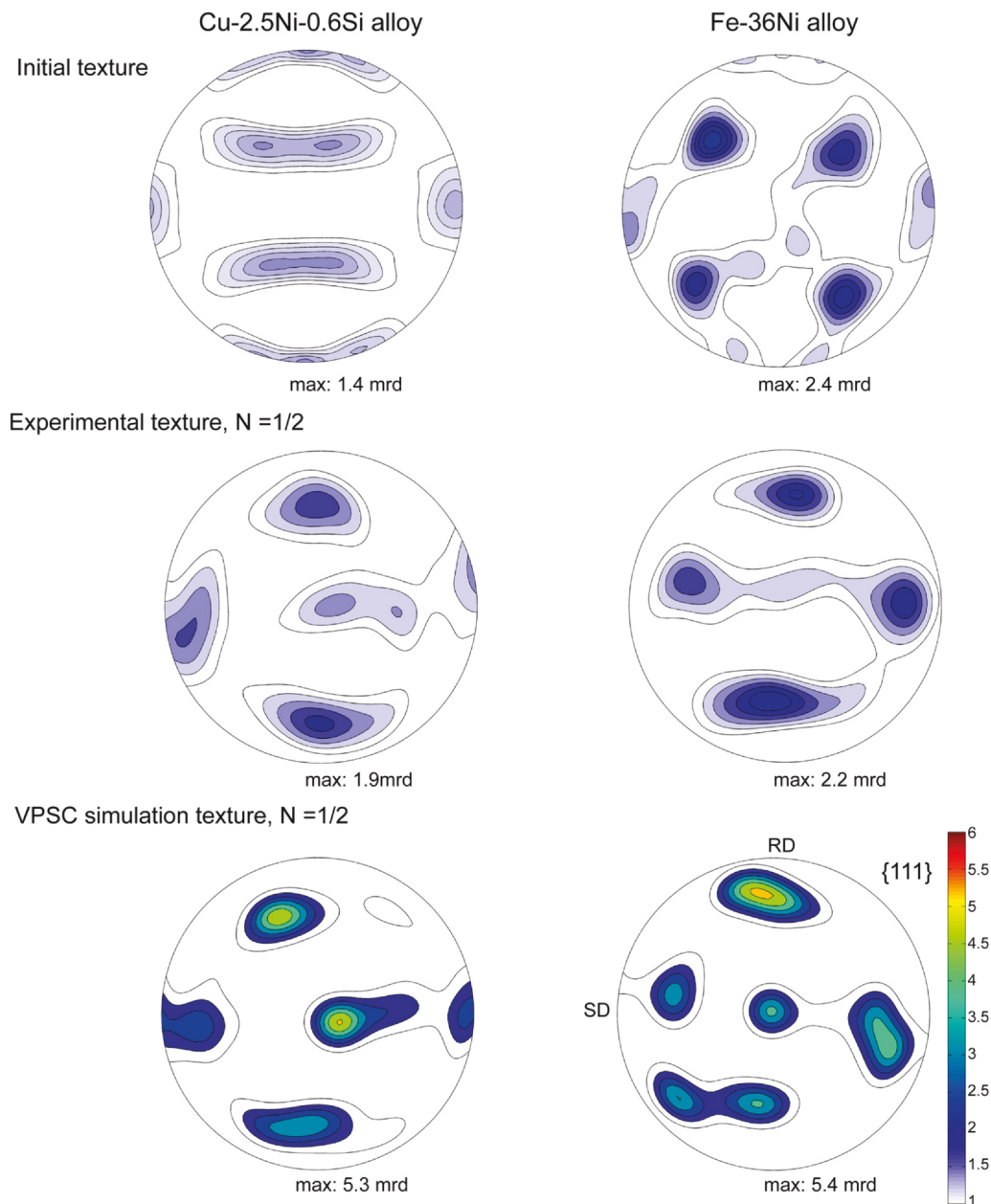H. Azzeddine, T. Baudin, A.-L. Helbert et al.

Fig. 6. Experimental and VPSC simulated texture after HPT processing for N = 1/2 turn showing the effect of the initial texture.

The rapid softening observed in the Fe-36Ni alloy is explained by the grain refinement mechanism in alloys with high γ_{SFE}. During the initial stage of HPT processing, the dislocation density increases and the dislocations accumulate to form dislocation cells and/or low-angle grain boundaries (LAGBs) and then they gradually transform to high-angle grain boundaries (HAGBs) through dislocation re-arrangement with increasing numbers of HPT turns. This is in good agreement with the microstructural evolution presented in Figs. 3 and 4 where the fraction of DRX in both alloys increases with increasing numbers of HPT turns. By contrast, the Cu-2.5Ni-0.6Si alloy shows a general strain hardening behavior and the slow annihilation of dislocations during deformation processing produces a smaller grain size as reported for low γ_{SFE} alloys [33]. It should be noted that a smaller grain size was reported in Cu-2.5Ni-0.6Si (~0.2 μm after N = 10 turns) [5] compared with Fe-36Ni (~0.37 μm after N = 10 turns) [6]. It is worth noting also that such softening behavior, due to the advent of rapid microstructural recovery, was first reported in an HPT-processed high purity Al with high γ_{SFE} [39] while most metals

and alloys including Cu alloys [40,41] demonstrate a hardness model of strain hardening without microstructural recovery with increasing numbers of HPT turns. These separate hardness models were more recently summarized and categorized for a variety of metals and alloys processed by HPT [42].

The grain refinement mechanism is often accompanied by a variation in grain boundary misorientation. Accordingly, Table 3 summarizes the evolution of the fraction of sub-grain boundaries (2–5°), LAGBs (5–15°) and HAGBs (> 15°) in the shear components for the Cu-2.5Ni-0.6Si and Fe-36Ni alloys after HPT processing at N = 10 turns. A detailed inspection shows that all shear components contain high fractions of sub-grain boundaries ranging from ~69–75% for both alloys after 10 turns. It is expected that the new fine grains will further deform and accumulate dislocations due to the continuous HPT processing. However, both alloys show a difference in the fractions of LAGBs and HAGBs. Specifically, the shear components of the Cu-2.5Ni-0.6Si alloy contain high fractions of LAGBs of ~23–26% while the shear components of the Fe-36Ni alloy exhibit higher fractions of HAGBs of ~13–18% compared with ~2.6–4.6% of HAGBs in

Table 3
Evolution of fraction (as a percentage) of different grain boundary misorientations in the shear components for Cu-2.5Ni-0.6Si and Fe-36Ni alloys after HPT processing for $N = 10$ turns.

	A_1^*	A_2^*	A	$\bar{A}$	B	$\bar{B}$	C
Cu-2.5Ni-0.6Si							
2–5° (%)	71.0	69.0	71.2	73.9	71.2	74.0	72.7
5–15°(%)	24.8	26.4	25.2	23	24.7	23.4	24.4
> 15°(%)	4.2	4.6	3.7	3.2	4.1	2.6	2.9
Fe-36Ni							
2–5°(%)	69.9	75.3	72.1	74.8	63.8	63.8	68.6
5–15°(%)	15.1	11.6	13.2	12.2	18.5	18.1	17.0
> 15°(%)	15.0	13.1	14.7	13.0	17.7	18.0	14.4

the Cu-2.5Ni-0.6Si alloy. This confirms the rapid formation of new fine grains with HAGBs in the Fe-36Ni alloy while the LAGBs require longer times for transformation to HAGBs in the Cu-2.5Ni-0.6Si alloy.

5. Summary and conclusions

- The correlation between the stored energy and the shear texture components of Cu-2.5Ni-0.6Si and Fe-36Ni alloys was investigated after HPT processing up to 10 turns at ambient temperature using the KAM approach.
- A typical stable shear texture developed for the Cu-2.5Ni-0.6Si alloy after 1 turn while a continuous transformation of the texture was observed in the Fe-36Ni alloy up to 10 turns. The texture difference between these two alloys is associated with differences in the γ_{SFE} and in the initial textures.
- HPT processing produced approximately the same amount of stored energy in the different shear texture components (~35 J/mol) for the Cu-2.5Ni-0.6Si alloy and lower values (~24 J/mol) for the Fe-36Ni alloy. There was no apparent hierarchy between these components.
- The stored energy in all shear components for the Cu-2.5Ni-0.6Si alloy increased with increasing processing to $N = 1$ turn and then slightly decreased up to $N = 10$ turns whereas the stored energy of the Fe-36Ni alloy continuously decreased with increasing numbers of HPT turns. These differences are related to the grain refinement mechanism during HPT processing.

CRediT authorship contribution statement

Hiba Azzeddine: Conceptualization, Investigation, Writing - original draft. **Thierry Baudin**: Visualization, Validation. **Anne-Laure Helbert**: Visualization, Validation. **François Brisset**: Software. **Yi Huang**: Investigation. **Megumi Kawasaki**: Investigation. **Djamel Bradai**: Conceptualization, Writing - original draft. **Terence G. Langdon**: Writing - review & editing.

Declaration of Competing Interest

The authors declare that they have no known competing financial interests or personal relationships that could have appeared to influence the work reported in this paper.

Acknowledgements

References

[1] F. Kocks, C. Tomé, H.R. Wenk, Texture and Anisotropy: Preferred Orientations in Polycrystals and Their Effect on Material Properties, Cambridge University Press, Cambridge, U.K, 1998.

[2] L.A.I. Kestens, H. Pirgazi, Texture formation in metal alloys with cubic crystal structures, Mater. Sci. Technol. 32 (13) (2016) 1303–1315.

[3] K. Tirsatine, H. Azzeddine, T. Baudin, A.-L. Helbert, F. Brisset, B. Alili, D. Bradai, Texture and microstructure evolution of Fe–Ni alloy after accumulative roll bonding, J. Alloy. Compd. 610 (2014) 352–360.

[4] I.J. Beyerlein, L.S. Tóth, Texture evolution in equal-channel angular extrusion, Prog. Mater. Sci. 54 (4) (2009) 427–510.

[5] A.Y. Khereddine, F. Hadj Larbi, H. Azzeddine, T. Baudin, F. Brisset, A.-L. Helbert, M.-H. Mathon, M. Kawasaki, D. Bradai, T.G. Langdon, Microstructures and textures of a Cu–Ni–Si alloy processed by high-pressure torsion, J. Alloy. Compd. 574 (2013) 361–367.

[6] K. Tirsatine, H. Azzeddine, Y. Huang, T. Baudin, A.-L. Helbert, F. Brisset, D. Bradai, T.G. Langdon, An EBSD analysis of Fe–36%Ni alloy processed by HPT at ambient and a warm temperature, J. Alloy. Compd. 753 (2018) 46–53.

[7] I.V. Gervas'eva, D.P. Rodionov, Y.V. Khlebnikova, V.A. Kazantsev, Formation of texture in thin tapes of Fe-Ni alloys during cold rolling and recrystallization, Phys. Met. Metallogr. 111 (3) (2011) 271–280.

[8] H. Wei, Y.-l Chen, L. Su, D. Tang, Z.-j Xu, Study on texture evolution and deformation mechanism of the Cu-Ni-Si alloy during cold-rolling treatment, Procedia Eng. 207 (2017) 1111–1116.

[9] B. Alili, D. Bradai, M.-H. Mathon, S. Jakani, T. Baudin, On the rolling and annealing texture in a Cu-15Ni-8Sn (wt%) alloy, Kov. Mater. 46 (2008) 371–376.

[10] A. Wauthier-Monnin, T. Chauveau, O. Castelnau, H. Réglé, B. Bacroix, The evolution with strain of the stored energy in different texture components of cold-rolled IF steel revealed by high resolution X-ray diffraction, Mater. Charact. 104 (2015) 31–41.

[11] H. Azzeddine, K. Tirsatine, T. Baudin, M.-H. Mathon, A.-L. Helbert, F. Brisset, D. Bradai, On the stored energy evolution after accumulative roll-bonding of invar alloy, Mater. Chem. Phys. 201 (2017) 408–415.

[12] A.L. Etter, M.H. Mathon, T. Baudin, V. Branger, R. Penelle, Influence of the cold rolled reduction on the stored energy and the recrystallization texture in a Fe–53%Ni alloy, Scr. Mater. 46 (4) (2002) 311–317.

[13] M.F. Ashby, The deformation of plastically non-homogeneous materials, Philos. Mag. A J. Theor. Exp. Appl. Phys. 21 (170) (1970) 399–424.

[14] G. Guiglionda, A. Borbély, J.H. Driver, Orientation-dependent stored energies in hot deformed Al–2.5%Mg and their influence on recrystallization, Acta Mater. 52 (12) (2004) 3413–3423.

[15] Y. Ateba Betanda, A.-L. Helbert, F. Brisset, M.-H. Mathon, T. Waeckerlé, T. Baudin, Measurement of stored energy in Fe–48%Ni alloys strongly cold-rolled using three approaches: neutron diffraction, Dillamore and KAM approaches, Mater. Sci. Eng. A 614 (2014) 193–198.

[16] H. Azzeddine, Y.I. Bourezg, A.Y. Khereddine, T. Baudin, A.-L. Helbert, F. Brisset, M. Kawasaki, D. Bradai, T.G. Langdon, An investigation of the stored energy and thermal stability in a Cu–Ni–Si alloy processed by high-pressure torsion, Philos. Mag. 100 (6) (2020) 688–712.

[17] J.J. Jonas, L.S. Tóth, Modelling oriented nucleation and selective growth during dynamic recrystallization, Scr. Metall. Mater. 27 (11) (1992) 1575–1580.

[18] S. Naghdy, L. Kestens, S. Hertelé, P. Verleysen, Evolution of microstructure and texture in commercial pure aluminum subjected to high pressure torsion processing, Mater. Charact. 120 (2016) 285–294.

[19] H. Beladi, P. Cizek, P.D. Hodgson, Texture and substructure characteristics of dynamic recrystallization in a Ni–30%Fe austenitic model alloy, Scr. Mater. 61 (5) (2009) 528–531.

[20] H. Beladi, P. Cizek, P.D. Hodgson, Dynamic recrystallization of austenite in Ni-30 Pct Fe model alloy: microstructure and texture evolution, Metall. Mater. Trans. A 40 (5) (2009) 1175–1189.

[21] Y. Takayama, J.A. Szpunar, Stored energy and taylor factor relation in an Al-Mg-Mn alloy sheet worked by continuous cyclic bending, Mater. Trans. 45 (7) (2004) 2316–2325.

[22] C. Fressengeas, B. Beausir, C. Kerisit, A.-L. Helbert, T. Baudin, F. Brisset, M.-H. Mathon, R. Besnard, N. Bozzolo, On the evaluation of dislocation densities in pure tantalum from EBSD orientation data, Matér. Tech. 106 (6) (2018) 604.

[23] R.B. Figueiredo, P.R. Cetlin, T.G. Langdon, Using finite element modeling to examine the flow processes in quasi-constrained high-pressure torsion, Mater. Sci. Eng. A 528 (28) (2011) 8198–8204.

[24] Y. Mikami, K. Oda, M. Kamaya, M. Mochizuki, Effect of reference point selection on microscopic stress measurement using EBSD, Mater. Sci. Eng. A 647 (2015) 256–264.

[25] F. Bachmann, R. Hielscher, H. Schaeben, Texture analysis with MTEX – free and open source software toolbox, Solid State Phenom. 160 (2010) 63–68.

[26] R. Badji, T. Chauveau, B. Bacroix, Texture, misorientation and mechanical anisotropy in a deformed dual phase stainless steel weld joint, Mater. Sci. Eng. A 575 (2013) 94–103.

[27] Y. Takayama, J.A. Szpunar, H. Kato, Analysis of intragranular misorientation related to deformation in an Al-Mg-Mn Alloy, Mater. Scie. Forum 495–497 (2005) 1049–1054.

[28] J.-H. Cho, A.D. Rollett, K.H. Oh, Determination of a mean orientation in electron backscatter diffraction measurements, Metall. Mater. Trans. A 36 (12) (2005) 3427–3438.

[29] R.E. Schramm, R.P. Reed, Stacking fault energies of fcc fe-Ni alloys by x-ray diffraction line profile analysis, Metall. Trans. A 7 (3) (1976) 359–363.

[30] P.C.J. Gallagher, The influence of alloying, temperature, and related effects on the stacking fault energy, Metall. Trans. 1 (9) (1970) 2429–2461.

[31] A. Khereddine, F.H. Larbi, L. Djebala, H. Azzeddine, B. Alili, D. Bradai, X-ray diffraction analysis of cold-worked Cu-Ni-Si and Cu-Ni-Si-Cr alloys by Rietveld method, Trans. Nonferrous Met. Soc. China 21 (3) (2011) 482–487.

[32] A.Y. Khereddine, F.H. Larbi, M. Kawasaki, T. Baudin, D. Bradai, T.G. Langdon, An examination of microstructural evolution in a Cu–Ni–Si alloy processed by HPT and ECAP, Mater. Sci. Eng. A 576 (2013) 149–155.

[33] Y.H. Zhao, X.Z. Liao, Y.T. Zhu, Z. Horita, T.G. Langdon, Influence of stacking fault energy on nanostructure formation under high pressure torsion, Mater. Sci. Eng. A 410–411 (2005) 188–193.

[34] X.H. An, S.D. Wu, Z.G. Wang, Z.F. Zhang, Significance of stacking fault energy in bulk nanostructured materials: Insights from Cu and its binary alloys as model systems, Prog. Mat. Sci. 101 (2019) 1–45.

[35] C. Tome, G.R. Canova, U.F. Kocks, N. Christodoulou, J.J. Jonas, The relation between macroscopic and microscopic strain hardening in F.C.C. polycrystals, Acta Metall. 32 (10) (1984) 1637–1653.

[36] A. Molinari, G.R. Canova, S. Ahzi, A self consistent approach of the large deformation polycrystal viscoplasticity, Acta Metall. 35 (12) (1987) 2983–2994.

[37] R.Z. Valiev, Y.V. Ivanisenko, E.F. Rauch, B. Baudelet, Structure and deformaton behaviour of Armco iron subjected to severe plastic deformation, Acta Mater. 44 (12) (1996) 4705–4712.

[38] Z. Hegedűs, J. Gubicza, M. Kawasaki, N.Q. Chinh, Z. Fogarassy, T.G. Langdon, Microstructure of low stacking fault energy silver processed by different routes of severe plastic deformation, J. Alloy. Compd. 536 (2012) S190–S193.

[39] C. Xu, Z. Horita, T.G. Langdon, The evolution of homogeneity in processing by high-pressure torsion, Acta Mater. 55 (1) (2007) 203–212.

[40] H. Jiang, Y.T. Zhu, D.P. Butt, I.V. Alexandrov, T.C. Lowe, Microstructural evolution, microhardness and thermal stability of HPT-processed Cu, Mater. Sci. Eng. A 290 (1) (2000) 128–138.

[41] Y.Z. Tian, S.D. Wu, Z.F. Zhang, R.B. Figueiredo, N. Gao, T.G. Langdon, Microstructural evolution and mechanical properties of a two-phase Cu–Ag alloy processed by high-pressure torsion to ultrahigh strains, Acta Mater. 59 (7) (2011) 2783–2796.

[42] M. Kawasaki, Different models of hardness evolution in ultrafine-grained materials processed by high-pressure torsion, J. Mater. Sci. 49 (1) (2014) 18–34.